Applied Catalysis B: Environmental 142–143 (2013) 817–827

Contents lists available at SciVerse ScienceDirect

Applied Catalysis B: Environmental

journal homepage: www.elsevier.com/locate/apcatb

Synthesis and characterization of large pore cubic mesoporous silicas functionalized with high contents of carboxylic acid groups and their use as adsorbents

Wei-Chieh Chang[a], Juti Rani Deka[a], Hao-Yiang Wu[b], Fa-Kuen Shieh[a,*], Shu-Ying Huang[a], Hsien-Ming Kao[a,**]

[a] Department of Chemistry, National Central University, Chung-Li 32054, Taiwan, ROC
[b] Department of Neurological Surgery, Tri-Service General Hospital National Defense Medical Center, 325, Sec. 2, Cheng-Kung Rd, Nei-Hu Dist, Taipei 11490, Taiwan, ROC

ARTICLE INFO

Article history:
Received 11 March 2013
Received in revised form 3 June 2013
Accepted 18 June 2013
Available online 27 June 2013

Keywords:
Carboxylic acid functionalization
Cubic mesoporous silica
Methylene blue
Paraquat

ABSTRACT

Well-ordered cubic FDU-12 type mesoporous silicas functionalized with various contents of carboxylic acid group (—COOH), up to 40 mol% based on silica, were synthesized via co-condensation of tetraethyl orthosilicate (TEOS) and carboxyethylsilanetriol sodium salt (CES) under acidic conditions using Pluronic F127 triblock copolymer as template. The materials thus obtained were characterized by a variety of techniques including powder X-ray diffraction (XRD), nitrogen adsorption–desorption, transmission electron microscopy (TEM), ^{13}C and ^{29}Si solid-state nuclear magnetic resonance (NMR) measurements. The materials were used as adsorbents for removal of methylene blue (MB) in aqueous solutions and as an antidote for intoxication of herbicide paraquat (PQ). Due to the —COOH functionalization, three-dimensional pores, high surface areas, and electrostatic interactions between the adsorbent and the adsorbates, the prepared adsorbents possessed very high adsorption capacities and extremely rapid rates for MB and PQ adsorption. The kinetic regression results revealed that the overall adsorption process was controlled by external mass transfer and intra-particle diffusion jointly. The Langmuir isotherm model showed better fit with the experimental adsorption data than the Freundlich isotherm model, implying a monolayer adsorption mechanism. The present results show that the prepared —COOH functionalized cubic mesoporous silicas have great potentials for removing pollutants and herbicides from aqueous solutions in environmental and clinical applications.

1. Introduction

The recent discovery of ordered mesoporous silica materials has opened prospects for the development of new technologies in catalysis, separation, drug delivery, and nanoscience, owing to their tunable size mesopores, high surface areas, versatile possibilities of surface functionalization, and diversity in composition, structure, and morphology [1–4]. Of particular current interest are mesoporous silicas consisting of three-dimensional (3D) interconnected cage-type large pores (e.g., pore diameter > 5 nm). Such types of cubic mesoporous silica materials are expected to be superior to two-dimensional (2D) hexagonal counterparts, especially for applications involving selectively tuned diffusion, immobilization of large molecules, or host–guest interactions within nanostructured materials as the 3D interconnected pores offer better pore accessibility than the cylindrical pores [5–9]. Several researchers have successfully synthesized ordered mesoporous materials with large pores, which possessed cubic structures with three-dimensional connectivity [10–13]. However, the applications of pure silica materials are limited due to their inherent catalytically inactive nature of mesopore surface. The surface properties of pure mesoporous silica materials are therefore needed to be modified by incorporating species with desired functionalities. It has been recognized that the content of functional organic groups plays a key role in governing many important properties of the hybrid materials [14], and therefore have wider applications including adsorption [15–17], catalysis [18–20], gas separation [21,22], drug delivery [23] and sensing [24]. Removal of organic pollutants from industrial and municipal wastewater is a great challenge to water suppliers worldwide [25–27]. The dying industry discharges organic pollutants and causes the increasing concern in environmental issues [28–30]. Dyes are generally non-degradable and constitute a problematic group of pollutants.

* Corresponding author.
** Corresponding author. Tel.: +886 3 4275054; fax: +886 3 4227664.
E-mail address: hmkao@cc.ncu.edu.tw (H.-M. Kao).

0926-3373/$ – see front matter © 2013 Elsevier B.V. All rights reserved.
http://dx.doi.org/10.1016/j.apcatb.2013.06.018

Methylene blue (MB), a heterocyclic aromatic chemical compound having IUPAC name 3,7-bis(dimethylamino)-phenothiazin-5-ium chloride with the molecular formula $C_{16}H_{18}N_3SCl$ [31] is the most commonly used substance for dying cotton, wood, and silk. However, it can cause eye burns and short period of rapid or difficult breathing on inhalation. In addition to those pollutants produced by textile industrial factories, overuse of herbicides is another constant source of worry to the environment, since herbicides give rise to toxicity and normally be persisted in soil due to less available for biological breakdown in the soil solution [32]. Besides that, herbicides are relatively cheaper, easily obtained and with acutely toxic so as to be used as "suicide agents" in some areas [33]. One particular herbicide, 1,1′-dimethyl-4,4′-bipyridinium dichloride, popularly known as paraquat (PQ), is a cationic non-systemic contact herbicide that has been worldwide used [34]. However, PQ is known to be extremely toxic and can result in a considerably higher fatality rate than other suicide chemicals, if accidentally ingested or purposely administered [35]. As an effective therapy for acute PQ poisoning has not yet been established, it is of great interest in the development of an effective adsorbent as antidote or filter for the removal of herbicides from poisoned circulation system or contaminated environment.

Many techniques have been developed to remove organic pollutants from aqueous solutions, including adsorption [17], ion-exchange [36], membrane filtration [37], and chemical oxidation [38]. Among the possible techniques, adsorption is one of the most promising and efficient techniques for removal of trace amount of contaminants in wastewater due to low cost, high efficiency and simplicity of the technique. Activated carbon has been widely used for this purpose because of its high adsorption capacity. However, the high cost of production and regeneration make it uneconomical. Therefore, inorganic adsorbents with high surface areas have been used as alternatives to carbon-based adsorbents [39–41]. For example, mesoporous materials MCM-41 [42] and SBA-15 [43] have been investigated for the removal of dyes from aqueous solutions and they showed effective adsorption performance because of large pore size, high surface area, and the interaction between the basic dye and surface hydroxyl groups.

The surface modification of mesoporous silica is an essential requirement in order to generate sufficient binding affinity for the material to be used for adsorption. A selective surface functionalization can introduce positive/negative charges on the silica surface, which in turn permits electrostatic interactions between the adsorbent and the adsorbates. Carboxylic acid group (—COOH) is an important functional group in organic chemistry, and can be easily deprotonated in neutral and basic environments to form negatively charged moieties. The formed negative moieties in the prepared silicas can be used as synthetic ion channels, acidic catalysts and for removing the cationic species from aqueous solutions as well [44–46]. The —COOH functionalized mesoporous silicas were used for dye removal, and the removal efficiencies were determined to be much higher than the non-functionalized mesoporous silicas [47–49]. Recently, we have reported the application of —COOH functionalized benzene-bridged periodic mesoporous organosilicas (PMOs) for efficient removal of MB [50]. The exceptionally high loadings of —COOH, up to 80ymol% based on silica, have increased the adsorption capacity and adsorption rate tremendously. Cage-like cubic porous structure is reported to be superior to the hexagonal structures such as MCM-41 and SBA-15, in terms of mass transfer and pore blocking [51]. Considering the advantages associated with the cubic mesostructure, in this study the effort was devoted to the synthesis of well ordered —COOH functionalized cage-like mesoporous silicas with large pores via co-condensation tetraethoxysilane (TEOS) and carboxyethylsilanetriol sodium salt (CES) under acidic conditions using Pluronic F127 triblock copolymer as template. The synthesized materials were then used as adsorbents for adsorption of MB, a cationic dye, and herbicide PQ from aqueous solutions. The —COOH group is believed to provide the silica surface with a sufficient quantity of negative charges to achieve relatively strong interactions with MB and PQ. To the best of our knowledge, there is no detailed study on the synthesis of large pore cage-like mesoporous silicas functionalized with high contents of —COOH moieties and their applications for adsorption of MB and PQ. The present work demonstrates that large pore cubic mesoporous silicas functionalized with —COOH groups are promising candidates for removing pollutants and herbicides from aqueous solutions in environmental and clinical applications.

2. Experimental

2.1. Materials

TEOS, F127 and MB were received from Sigma–Aldrich. CES (25 wt.% in water) was purchased from Gelest. PQ was obtained from ACROS organic. All chemicals were used as received without any further purification.

2.2. Sample preparation

The synthesis procedures of FDU-12 type cubic mesoporous silica materials were modified slightly according to the previously reported literature [10]. In a typical synthesis of —COOH functionalized large pore mesoporous silicas, non-ionic copolymer surfactant F127 (1.0 g) and the pore expander 1,3,5-trimethylbenzene (TMB) (1.0 g) were dissolved in HCl (60.0 mL, 2 M) mixed with KCl (2.5 g). The solution was stirred at room temperature for 24 h. A premixed solution of TEOS and CES was then added dropwise to the above mixture under vigorous stirring and the solution was stirred continuously for another 24 h at 40 °C. The reaction mixture was treated hydrothermally at 100 °C for 72 h. The resultant white precipitate was filtered, washed with water and dried at 70 °C. The molar composition of the reaction mixture was $(1-x)$/100 TEOS: x/100 CES: 0.004 F127: 6 HCl: 139 H_2O: 0.42 TMB: 1.7 KCl, where x is the molar percentage ratio of CES/(TEOS + CES). The template was removed from the as-synthesized materials (0.5 g) by adding H_2SO_4 (100.0 g, 48 wt.%) and heating the mixture at 90 °C for 24 h. The product was then filtered and washed with acetone. To completely remove any ester groups that might have formed during the treatment with H_2SO_4, the material (0.3 g) was re-treated with 2 M HCl (30.0 mL). Subsequently, the sample was recovered by washing with water and dried at ambient temperature. The final products were denoted as FTC-x, where x represents the molar percentage ratio of CES/(TEOS + CES).

2.3. Adsorption equilibrium experiments

2.3.1. MB adsorption

The FTC-x adsorbents were tested for adsorption of MB and PQ. To perform the MB adsorption experiments, FTC-x (4.0 g) was first dispersed in the MB solution (5 mL) and shaken at 25 °C in 300 rpm using a rotating oscillator incubator. The solution was then centrifuged to separate the adsorbed dye and the residual amount of dye in the solution was measured at 292 and 664 nm for MB using a UV-Vis spectrometer (SP-722). The amount of dye adsorbed (Q_e) was calculated using the equation,

$$Q_e = \left[\frac{(C_0 - C_e) \times V}{m}\right] \quad (1)$$

where C_0 and C_e are the initial and equilibrium concentrations of the dye solution (mg/L), V is the volume (L), and m is the adsorbent

mass (g). The adsorption equilibrium experiments were carried out at the optimized pH value at 25 °C with four different initial concentrations (100, 166, 214 and 250 ppm) of MB. The influence of pH in the adsorption process was studied by varying the pH of the dye solution from 2 to 9. To study the effect of the contact time, FTC-*x* (0.4 g) was dispersed in the MB solution (250 ppm, pH = 9) and shaken for different time intervals. The solution was withdrawn at a predetermined time, and the concentration of the residual amount of dye was then determined.

2.3.2. Desorption of MB

Experiments were conducted in order to assess the regeneration properties of the FTC-30. Adsorbents (0.2 g) were added to MB (20 mg/L) at pH 9 and kept for 12 h at 30 °C. The dye adsorbed samples were suspended in HCl (2 M) and ultrasonically treated for 3 h to desorb the dye. After desorption, the recovered adsorbent was thoroughly washed with deionized water until a neutral pH was obtained. To be reused in the next cycle of adsorption experiments the regenerated material was then dried and suspended in dye solution. The adsorption–desorption cycle was repeated up to five times.

2.3.3. Paraquat adsorption

The PQ adsorption tests were carried out in a 20 mL screw cap sample vial. FTC-*x* (1.0 g) was dispersed in the PQ solution (20.6 ppm), and the mixture was incubated for 1 h. The vials were shaken on a Lab-Line orbital shaker (200 rpm) for 2 h at 25 °C. The solutions were then centrifuged, and the collected supernatant was filtered through Millex syringe-driven PTFE filters (0.22 m). The change in concentration of PQ was checked with a UV-Vis spectrometer (S-3100) at a wavelength of 258 nm. The PQ removal efficiencies of the adsorbents were determined from the UV adsorption peak of PQ aqueous solution with or without the adsorbent using the following relationship,

$$\text{Removal efficiency}\,(\%) = \left[\frac{(C_P - C_F)}{C_p} \times 100\%\right] \quad (2)$$

where C_F is the concentration of the PQ recovered in the supernatant after absorbed by FTC-*x* and C_P is the concentration of the standard PQ solutions. The pH of the PQ solution was maintained at 7 by using sodium phosphate buffer (10 mM).

2.4. Characterization methods

Powder X-ray diffraction (XRD) patterns were collected on Wiggler-A beamline (λ = 0.133367 nm) at the National Synchrotron Radiation Research Center in Taiwan. N_2 adsorption–desorption isotherms were measured at 77 K on a Micromeritics ASAP 2020 analyzer. The samples were degassed at 180 °C for several hours before measurements. The Brunauer–Emmett–Teller (BET) method in the relative pressure range of $P/P_0 = 0.05–1.0$ was employed to obtain specific surface areas. The sizes for the cage and the entrance were determined from the analysis of the adsorption and desorption branches of the isotherms, respectively, by the Barrett–Joyner–Halenda (BJH) method. Pore volumes were obtained from the volumes of N_2 adsorbed at $P/P_0 = 0.95$ or in the vicinity. Thermogravimetric analysis (TGA) was performed using a Perkin-Elmer TGA 7 apparatus at a heating rate of 10 °C/min under an air flow. Transmission electron microscopy (TEM) was carried out on a JEOL JEM2100 microscope operating at 160 kV. Solid-state ^{13}C and ^{29}Si NMR spectra were recorded on a Varian Infinityplus-500 NMR spectrometer, equipped with 5.0 and 7.5 mm Chemagnetics probes. The Larmor frequencies for ^{13}C and ^{29}Si nuclei are 125.7 and 99.3 MHz, respectively. ^{13}C cross-polarization magic angle spinning (CPMAS) NMR spectra were acquired at a spinning speed of 9 kHz and at a contact time of 1 ms. ^{29}Si MAS (magic angle spinning) NMR spectra were acquired with a recycle delay of 200 s. Both ^{13}C and ^{29}Si chemical shifts were externally referenced to tetramethylsilane (TMS) at 0 ppm.

3. Results and discussion

3.1. XRD study

It is well known that the organosilane concentration affects the mesoscopic order and pore size of the mesoporous materials prepared with the co-condensation method [2–4]. As the amount of organosilane increases, less ordered mesoporous materials are produced. The XRD patterns of the template-extracted FTC-*x* materials are shown in Fig. 1. The patterns show five well-resolved peaks for FTC-*x* (*x* = 0–50), which can be assigned to the (1 1 1), (2 2 0), (3 1 1), (3 3 1) and (4 4 2) reflections of a face-centered cubic structure, which are similar to the XRD pattern of FDU-12 reported in the literature [10]. The presence of strong diffraction peak of the (1 1 1) reflection, characteristics of $Fm\bar{3}m$ symmetry at 2θ below 0.5°, indicates the existence of long-range periodicity. However, the (2 2 0) peak disappeared and the intensity of the (1 1 1) peak decreased when the CES contents in the silicon sources were above 50%, suggesting the degradation of the long range periodicity upon increasing the CES contents. The structural degradation with the increase of CES content in the reaction mixture can be attributed to the different hydrolysis and condensation rates of the two structurally different precursors TEOS and CES. Another reason for the degradation of the mesostructure with the higher CES amount could be due to the difference in the anionic charge density on the wall surface, which hinders the formation of ordered mesostructures. During the synthesis, triol sites of CES co-condensed with the silica source TEOS and assembled to form the silica network. With the increase in CES, the amount of negatively charged carboxylate groups covalently bonded to the silica wall increases and causes difference in the charge density on the wall surface. This difference in anionic charge density affects the interaction between the surfactant micelle and silicate, and interrupts the pore development from the micelles, which leads to a less ordered mesostructure at a CES loading over 50%. The XRD peak positions were observed to be unaltered after the template removal, indicating no shrinkage of the cell dimensions of the materials. The unit cell parameter a_0 was determined from the d_{111} spacing and the results are summarized in Table 1. The EO/PO ratio and polymer architecture have also influence on the formation of the mesostructured silica. The EO/PO ratio < 0.07–1.5 favors the formation of hexagonal (*p*6*mm*) mesoporous silica and >1.5 gives cubic mesoporous silica [52]. We have recently reported the synthesis of carboxylate groups functionalized highly ordered SBA-15 via co-condensation TEOS and CES using P123 as the template, where 60 mol% CES (based on silica) was incorporated in the initial synthesis mixture without the expense of the integrity and the stability of pore structure [53]. Although the cubic mesostructure has many advantages in catalytic and many other applications compared with the hexagonal pore system, its structure formed only in a very narrow window in most cases. The highly ordered cubic mesoporous silica FDU-12 functionalized with 50 mol% CES synthesized in this study are expected to be promising for various applications.

3.2. Textural and structural studies

The nitrogen adsorption–desorption isotherms of FTC-*x* are shown in Fig. 2 and the corresponding structural properties are listed in Table 1. According to the IUPAC classification, the isotherms of FTC-*x* (0–40) are of type IV with H_2 hysteresis loops,

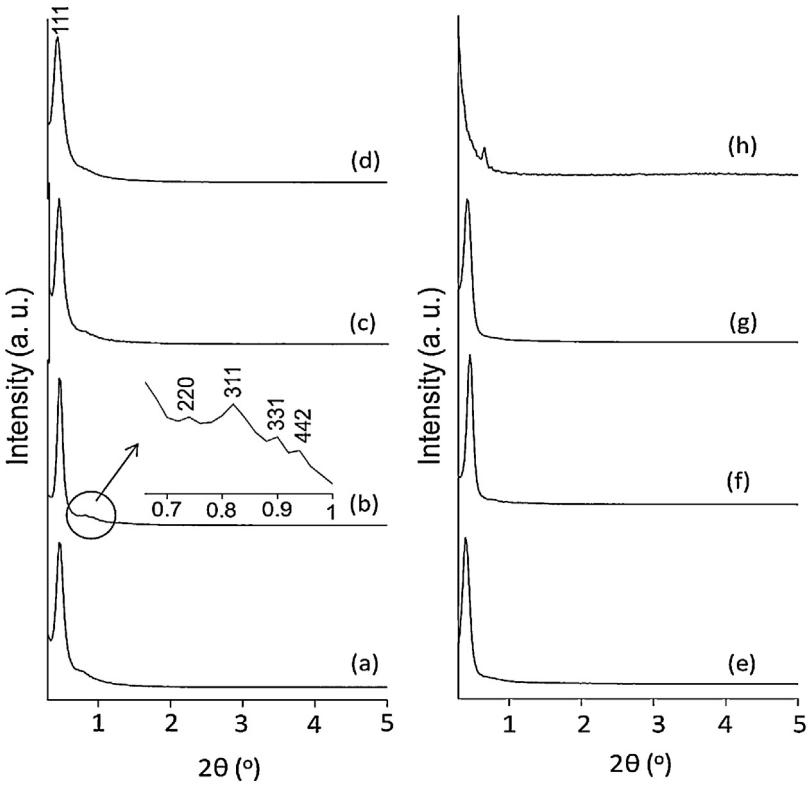

Fig. 1. Powder XRD patterns of template extracted FTC-*x*, where *x* = (a) 0, (b) 10, (c) 20, (d) 30, (e) 40, (f) 50, (g) 55, and (h) 60.

which indicate the existence of large mesopores [54]. However, the introduction of CES in the synthesis process leads to the decrease in specific surface area and pore volume, both of which are attributed to the occupation of the mesopores by the —COOH group in CES. Nevertheless, the surface area and pore volume appeared to be relatively high for —COOH loading up to 30%, but substantially decreased for the loading more than 40%. The hysteresis was also observed at a relative pressure from 0.15 to 0.9 when the CES content was 50% (FTC-50). The hysteresis loop of FTC-50 changed to the H_3 type, which indicated the presence of the slit shaped pores formed from with aggregation of plate-like particles [54]. The formation of well defined 3D cubic mesostructure was also confirmed by the TEM measurements. The representative TEM images of the template-extracted FTC-10 taken along the [1 1 1] and [1 0 0] directions are shown in Fig. 3a and b respectively. As shown in parts (c) and (d) of Fig. 3, nevertheless, both FTC-30 and FTC-40 exhibited wormlike mesostructures when the CES contents were high. The observed highly ordered lattice in the samples array suggested that the cubic pore structure and pore size were all well preserved for the functionalized materials.

3.3. FTIR and TGA studies

To qualitatively determine the amount of CES incorporated in FTC-x, FTIR and TGA measurements were conducted. Since the —COOH functional group exhibits a specific band around 1720 cm^{-1} in FTIR spectra, the appearance of this band is the direct evidence for the presence of the —COOH organic functionalities, and the corresponding intensities can serve as a guide of their relative abundance. Therefore, FTIR is useful to identify the presence of —COOH integrated into the silica framework. The FTIR spectra of FTC-*x* (*x* = 0–55), as shown in Fig. 4, show high intensity peaks at 948 and 3450 cm^{-1} for Si—OH groups and at 1076 cm^{-1} for the Si—O—Si linkage. An additional strong band at 1725 cm^{-1}, which is attributed to the —COOH group, is observed, except for the case of FTC-0. The intensity of this band is progressively increased with the increase in the CES contents, which confirms the successful incorporation of the —COOH functional group into the mesoporous silica framework.

TGA was employed to determine the thermal stability of the–COOH group within FTC-*x*. The TGA and DTA curves of as-synthesized (FTC-30) and template-extracted FTC-*x* (*x* = 0–50) are

Table 1
Structural and textural properties of FTC-*x*, where *x* represents the molar percentage ratio of CES/(TEOS + CES).

x	d_{111} (nm)	a_0 (nm)[a]	A_{BET} (m^2/g)[b]	V_p (cm^3/g)[c]	Cage size (nm)	Entrance size (nm)
0	16.6	28.8	906	0.91	11.2	4.0
10	16.6	28.8	647	0.73	9.2	3.8
20	16.6	28.8	698	1.19	9.2	3.9
30	17.4	30.1	377	0.74	11.2	3.7
40	19.1	33.1	197	0.26	9.2	3.9
50	16.6	28.8	96	0.38	7.6	3.9

[a] Lattice parameters a_0 were calculated based on the formula $a_0 = d_{111} \times \sqrt{3}$.
[b] A_{BET}: BET surface area.
[c] V_p: pore volume.

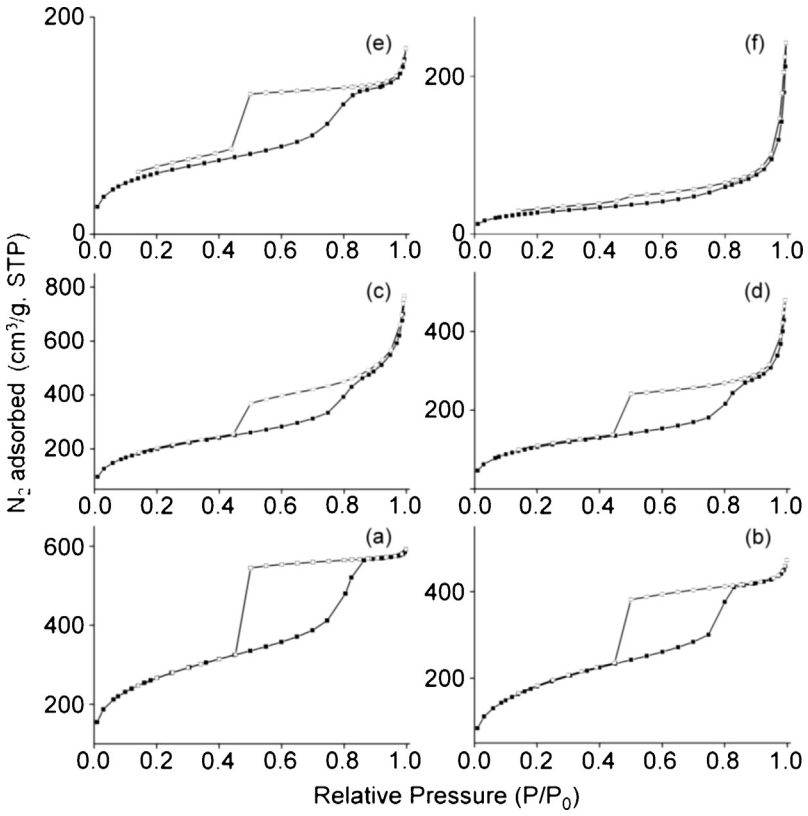

Fig. 2. N_2 adsorption–desorption isotherms of template extracted FTC-*x*, where *x* = (a) 0, (b) 10, (c) 20, (d) 30, (e) 40, and (f) 50.

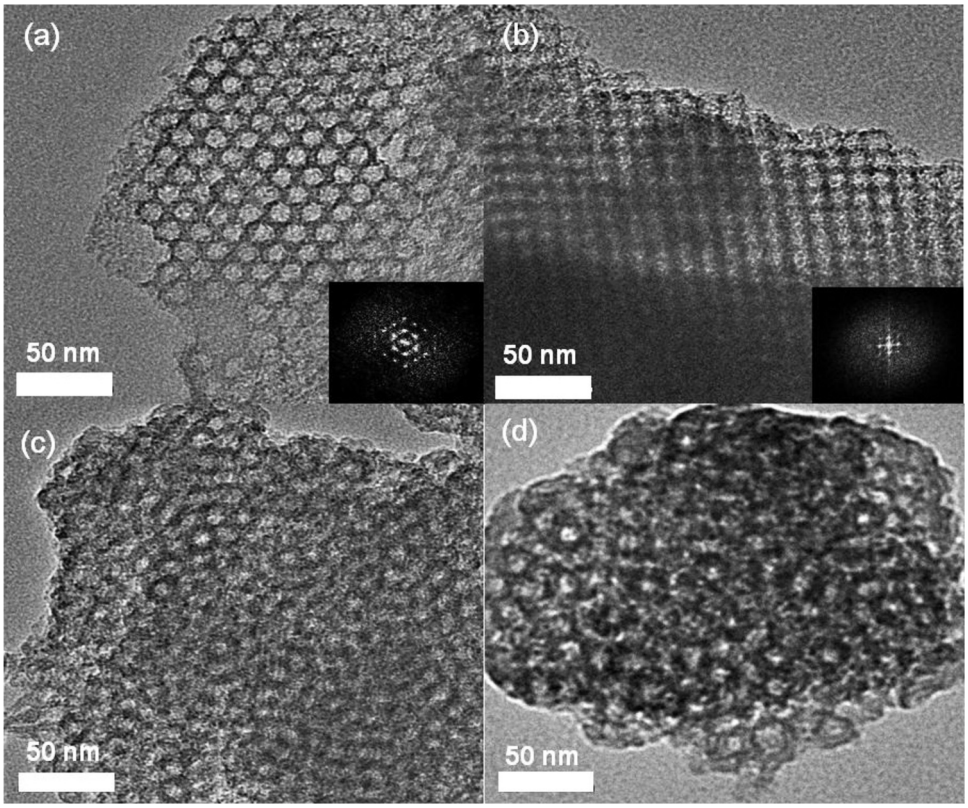

Fig. 3. TEM images of FTC-10 recorded along (a) [1 1 1] and (b) [1 0 0] directions (Fourier diffractograms inset); TEM images of (c) FTC-30, and (d) FTC-40 are also shown.

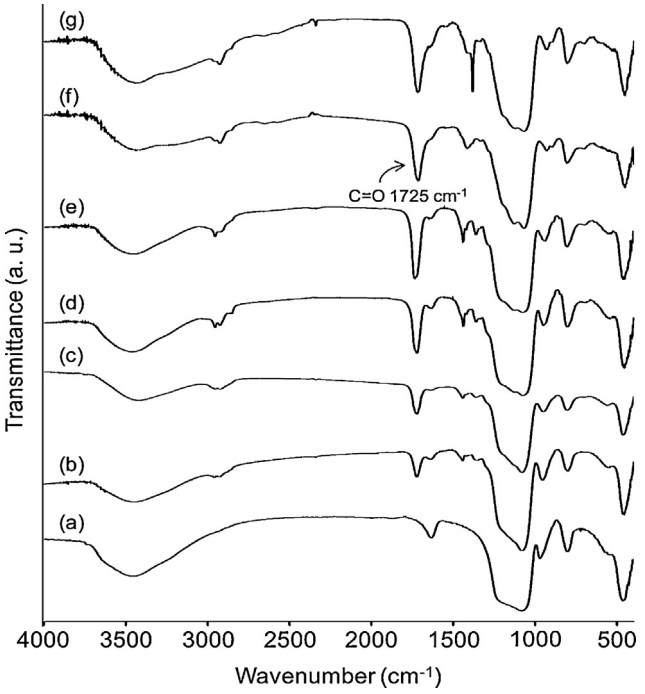

Fig. 4. IR spectra of template-extracted FTC-*x*, where *x* = (a) 0, (b) 10, (c) 20, (d) 30, (e) 40, (f) 50 and (g) 55.

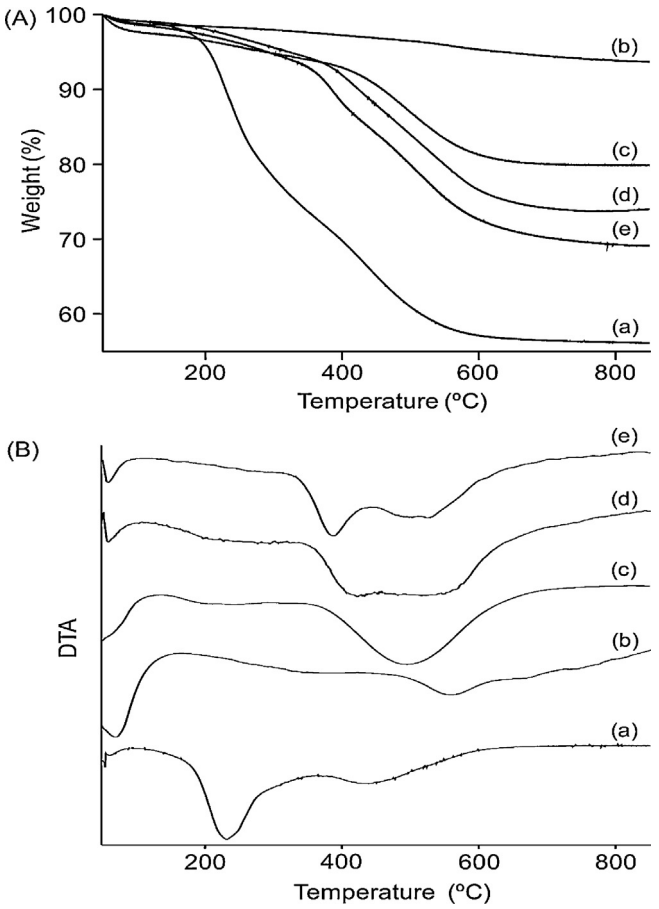

Fig. 5. (A) TGA and (B) DTA curves of (a) as-synthesized FTC-30, and template-extracted (b) FTC-0, (c) FTC-20, (d) FTC-30 and (e) FTC-50.

shown in Fig. 5A and B, respectively. The as-synthesized FTC-30 exhibited a weight loss of about 3% at temperatures lower than 180 °C, which can be attributed to the loss of small amounts of water adsorbed in the material. This initial weight loss was followed by weight loss of 12% in the temperature range of 180 to 310 °C due to the decomposition of the surfactant [55]. The significant weight loss of around 20% in the temperature range of 300 to 450 °C can be attributed to the decomposition of the–COOH groups [56]. At even higher temperatures around 450–600 °C, there was another weight loss of 6~8%, which most likely comes from further co-condensation of the silica matrix. The TGA curve of the template-extracted samples showed a similar weight loss pattern with the increase in temperature, except the significantly reduced weight loss of around 3% up to 300 °C, as expected after template removal. The total weight loss was progressively increasing with increase in the CES contents. The DTA curve showed an exothermic peak at around 430 °C for all the samples, which corresponds to the thermal decomposition of CES. This weight loss behavior demonstrated that FTC-*x* has high thermal stability and the functionalized–COOH groups preserved in the material up to 400 °C.

3.4. ^{13}C and ^{29}Si solid-state NMR studies

^{13}C and ^{29}Si solid-state NMR experiments were performed on the template-extracted FTC-*x* to confirm the successful incorporation of —COOH group in the silica framework. Fig. 6 shows the ^{13}C CPMAS NMR spectra of FTC-*x*. The peak at 7 ppm is attributed to the $—CH_2$ group (C3 carbon) directly bonded to the Si atom of the —COOH group due to CES. The presence of —COOH group can directly be judged from two distinct peaks with chemical shifts of 28 and 178 ppm. The resonance at 28 ppm is assigned to the $—CH_2$ carbon (C2 carbon) and at 178 ppm to —C=O carbon of the —COOH group, which confirm successful incorporation of the —COOH groups into the FTC-*x* materials. All these four ^{13}C CPMAS NMR spectra look similar because their signals all come from CES moiety solely. No other peaks due to the surfactant molecules are observed, indicative of complete surfactant removal.

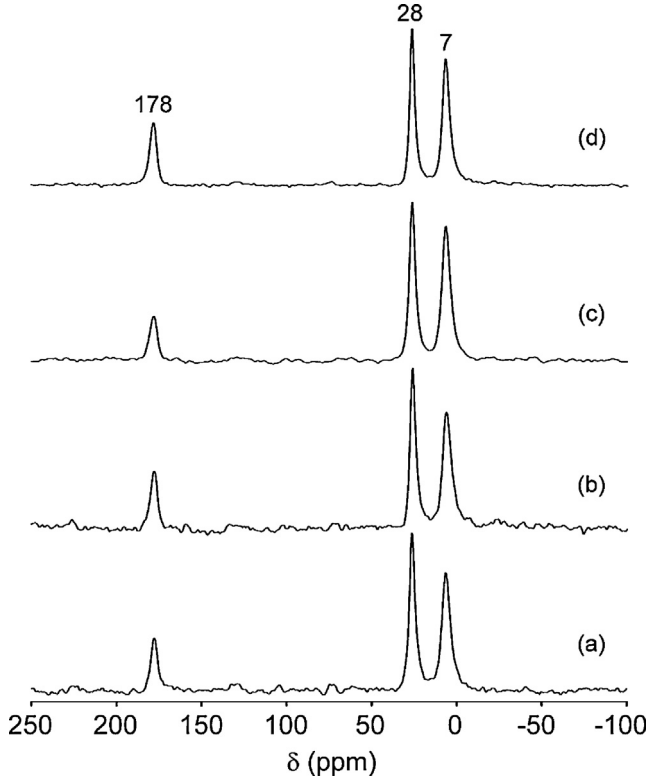

Fig. 6. ^{13}C CPMAS NMR spectra of template-extracted FTC-*x*, where *x* = (a) 10, (b) 20, (c) 40, and (d) 50.

Table 2
Deconvolution results of ^{29}Si MAS NMR for template-extracted FTC-*x*.

x	*Q*			*T*			$T^m/(Q^n+T^m)$ (%)
	Q^4 (%)	Q^3 (%)	Q^2 (%)	T^3 (%)	T^2 (%)	T^1 (%)	
20	64.3	12.5	2.2	20.2	0.7	0	20.9
40	50.7	9.9	0	24.1	9.5	5.8	39.7
50	49.9	16.3	0	42.5	4.6	0	47.1

The successful incorporation and loading of the functional groups into the silica framework can be identified and estimated by ^{29}Si MAS NMR. ^{29}Si NMR spectroscopy is a powerful tool to quantitatively determine the CES contents incorporated into FTC-*x* as the T and Q sites derived from CES and TEOS, respectively, exhibited distinct chemical shift ranges. As shown in Fig. 7, an intense peak at −110 ppm along with two shoulders peaks at −104 and −93 ppm are observed for the Q species in the spectra of the FTC-*x* (*x* = 10–50). The chemical shift at −110 ppm can be assigned to $Si(OSi)_4$ (Q^4, $Q^n = Si(OSi)_n(OH)_{4-n}$, $n \leq 4$) structural units, while the other peaks at −104 and −93 ppm can be compared to $Si(OSi)_3OH$ (Q^3) and $Si(OSi)_2(OH)_2$ (Q^2) structural units, respectively. The Q^4 structural units represent interlinked SiO_4 tetrahedrons in the interior of the mesopore walls, while Q^3 and Q^2 structural units are present on the wall surface associated with silanol groups [57]. Two resonance peaks related to the T species are also observed with chemical shifts of $\delta = -60$ ppm for T^2 and $\delta = -72$ ppm for T^3 species for FTC-20 and FTC-50. Apart from T^2 and T^3 species, the T^1 species at −50 ppm is also observed for FTC-40. The intensity of T group progressively increased with increasing the CES contents [54]. The relative integrated intensities of Q^n and T^m NMR signals allow the quantitative assessment of the degree of incorporation of the organic moiety. The $T^m/(T^m + Q^n)$ ratios are determined by deconvolution of each spectrum on the basis of the peak positions, and the results are summarized in Table 2, which is in close agreement with those expected based on the composition of the initial mixture.

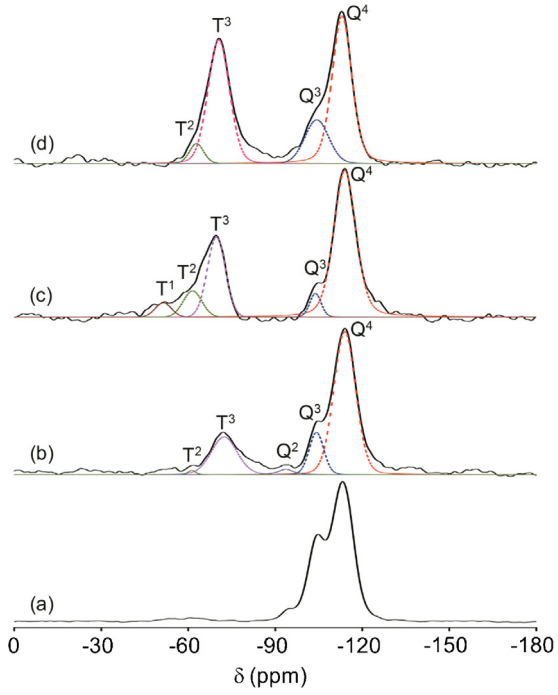

Fig. 7. ^{29}Si MAS NMR spectra of template-extracted FTC-*x*, where *x* = (a) 0, (b) 20, (c) 40, and (d) 50.

3.5. FTC-x as methylene blue adsorbent

3.5.1. Effect of initial pH

Adsorption of dye molecules onto an adsorbent is highly pH dependent since the functional groups, which are responsible for the interaction between the dye molecules and the adsorbent, can be protonated or deprotonated to produce different surface charges in solution at different pH values [58]. The effect of initial solution pH was studied in the range of 2–9 using FTC-30 as the adsorbent (Figure S1, Supplementary Information). The MB removal efficiency was increasing from 30% to 65% when the pH was from 2 to 9. The point of zero charge (pzc) of any adsorbent is a very important characteristic that determines the pH at which the surface has net electrical neutrality. It is well-known that for basic dye adsorption, negatively charged groups on the adsorbent are necessary. At lower pH, surface charge on the adsorbent may get positively charged due to the presence of H_3O^+ ions [59]. The electrostatic repulsion between the dye molecules and positively charged active sites on the adsorbent surface leads to a decrease in dye uptake at lower pH. However, as the surface charge density decreases with an increase in pH, the electrostatic repulsion between the positively charged dye molecule and the surface charge on the adsorbent was lowered, this may result in an increase in the adsorption capacity.

3.5.2. Effect of contact time and adsorption kinetics

Adsorption is a physiochemical process that involves mass transfer of a solute from the liquid phase to the adsorbent surface. Therefore, contact time has a profound influence on the MB dye uptake. Fig. 8 displays the effect of contact time on MB removal by FTC-*x*. The adsorption was rapid for all the samples in the initial 10 min period due to chemisorption, became slow with the increase in contact time (10–180 min), and then nearly reached a plateau after approximately 720 min. The slower adsorption rate in the range of 10–180 min can be attributed to the longer time period required by the dye molecules to access all the reactive sites due to the 3D cubic structure. Fig. 8 shows that FTC-30 exhibited a higher

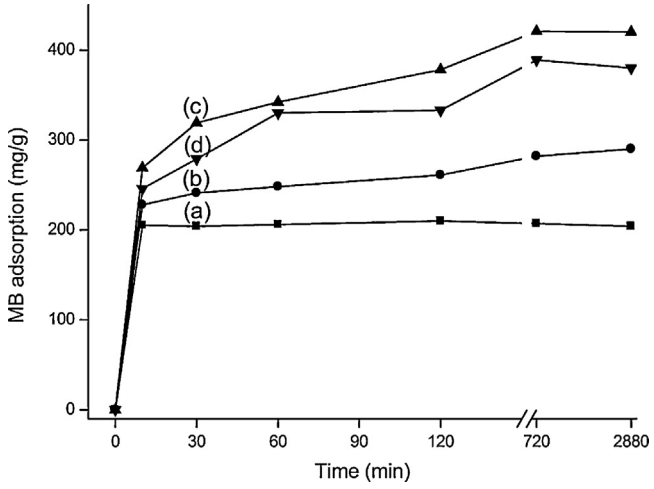

Fig. 8. Effect of contact time on the adsorption of MB onto (a) FTC-0, (b) FTC-10, (c) FTC-30, and (d) FTC-50.

Table 3
Kinetic parameters of pseudo-first order, pseudo-second order, and Weber–Morris models for methylene blue adsorption.

x	Pseudo-first order			Pseudo-second order			Weber–Morris		
	k_1 (min^{-1})	Q_e (mg/g)	R^2	k_2 (g/mg/min)	Q_e (mg/g)	R^2	k_{id} (mg/g/$min^{1/2}$)	R^2	C
0	0.00029	10.51	0.213	−0.0024	204.00	0.999	1.852	0.983	197
10	0.00333	76.27	0.800	0.0004	290.50	0.999	3.951	0.966	216
30	0.00699	137.00	0.964	0.0001	420.17	0.999	12.16	0.983	234
50	0.00091	120.85	0.843	0.0004	381.30	0.999	10.08	0.966	216

adsorption rate in comparison to the FTC-50 due to the high surface area, large pore size and ordered mesoporous structure of FTC-30 in addition to the presence of —COOH groups. However, the overall adsorption capacity FTC-*x* was significantly high. Despite poor ordered structure and low surface area, FTC-50 also exhibited a relatively high adsorption rate due to the presence of more negatively charged groups on its surface. It was also noted that the —COOH loaded samples adsorbed more dyes than the sample without the —COOH group (i.e., FTC-0). These observations indicate active participation of —COOH group in the adsorption process. The strong electrostatic interaction between the charged surface and the positively charged dye molecule is believed to be the main reason for its high adsorption capacity.

To identify the step possibly controlling the adsorption of MB onto FTC-*x*, the experimental data were fitted to three conventional kinetic models, including the pseudo-first order [60], pseudo-second order [61], and the intraparticle diffusion models [62]. The linear forms of these models are given as,

$$\text{Pseudo-first order equation :} \quad \ln(Q_e - Q_t) = \ln(Q_e) - k_1 t \tag{3}$$

$$\text{Pseudo-second order equation :} \quad \frac{t}{Q_t} = \frac{1}{k_2 Q_e^2} + \frac{t}{Q_e} \tag{4}$$

$$\text{Weber} - \text{Morris equation :} \quad Q_t = k_{id} t^{1/2} + C \tag{5}$$

where Q_e and Q_t are the amounts of dye adsorbed at equilibrium and at any time t, k_1 is the rate constant of the first order adsorption, k_2 is the rate constant of the second order equation, k_{id} is the rate constant of the intraparticle model and C is a constant. The rate constants k_1 and k_2 determined from the $\ln(Q_e - Q_t)$ versus t and t/Q_t versus t plots respectively are given in Table 3. The correlation coefficients (R^2) of the pseudo-second order were determined to be much higher than those of the pseudo-first order, and Q_e were closer to the experimental values (Table 4). Hence, chemisorption was supposed to be the rate limiting step in the adsorption process. To determine the rate-controlling step involved in the MB adsorption process more precisely, the experimental data were also fitted to Weber–Morris model and the resulting plot of Q_t versus $t^{1/2}$ is shown in Fig. 9. The intraparticle diffusion constant k_{id} was calculated from the slope of the linear portion of the plot and the values are presented in Table 3. Fig. 9 shows that the dye adsorption amount is not linear over the entire time range; instead it presents a multilinear behavior. The rapid adsorption rate in the initial stage is attributed to the external diffusion process. The second portion describes the diffusion of the adsorbate from the external surface into the pores of the adsorbent (pore or intraparticle diffusion) [59]. The slower adsorption rate herein is due to the difficulty in the occupation of the remaining surface sites owing to the repulsive forces between the solute molecules on the adsorbent and the bulk phases [63,64]. Therefore, intraparticle and boundary diffusions collectively control the adsorption process [65,66]. However, a correlation coefficient value close to 0.98 indicates significant contribution from intraparticle diffusion. The intraparticle diffusion rate was calculated to be highest for FTC-30.

Table 4
Saturated methylene blue adsorption capacities of FTC-*x*.

x	Q_{max} (mg/g)	Q_{max} (mmol/g)	Maximum adsorption per unit surface area (mmol/m^2)
0	184	0.49	0.0005
10	312	0.81	0.0013
30	374	1.00	0.0027
50	333	0.89	0.0093

3.5.3. *Effect of initial adsorbate concentration and adsorption isotherms*

The effect of initial dye concentration on the adsorption process was studied by varying the initial dye concentrations. Fig. 10A shows the equilibrium isotherms of MB adsorption onto FTC-*x*, and the saturated adsorption capacities of the adsorbents are given in Table 4. Adsorption isotherm models provide useful data in order to understand the adsorption mechanisms. Langmuir [67] and Freundlich [68] isotherm models were employed in this study to analyze the relationship between the amount of dye cations adsorbed onto FTC-*x* and their equilibrium concentrations in aqueous solution.

The linear form of Langmuir isotherm equation is,

$$\frac{C_e}{Q_e} = \frac{C_e}{Q_{max}} + \frac{1}{K_L Q_{max}} \tag{6}$$

where Q_e is the equilibrium amount of dye adsorbed on adsorbent (mg/g), C_e is the concentration of adsorbate under the equilibrium condition (mg/L), Q_{max} is the maximum amount of adsorbate adsorbed on adsorbent (mg/g) and K_L is the adsorption equilibrium constant (L/mg) [67]. The effect of the isotherm shape was also studied to understand which adsorption system was favorable. Another important parameter, R_L, called the separation factor or equilibrium parameter, which can be used to determine the feasibility of

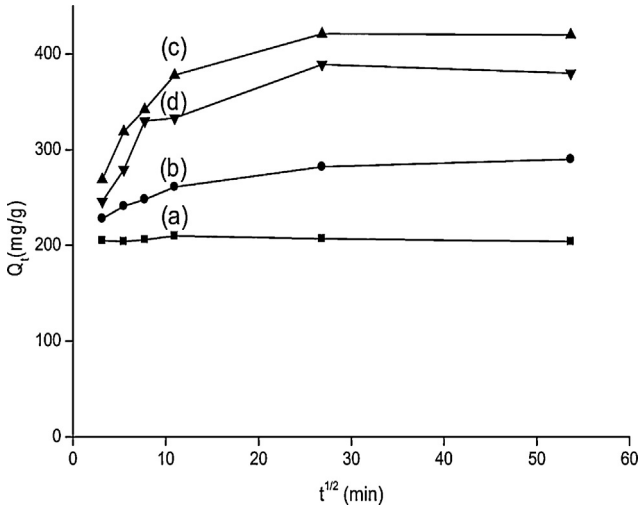

Fig. 9. Q_t versus $t^{1/2}$ plots for intraparticle diffusion model: (a) FTC-0, (b) FTC-10, (c) FTC-30, and (d) FTC-50 at pH = 9.

Table 5
Isotherm parameters for methylene blue adsorption on FTC-*x*.

x	Langmuir's parameters				Freundlich's parameters		
	K_L (L/mg)	Q_{max} (mg/g)	R^2	R_L	K_F ($mg^{(1-1/n)}L^{1/n}/g$)	*n*	R^2
0	3.92	189	0.999	0.001	0.35	8.92	0.978
10	1.15	321	0.995	0.004	0.62	11.95	0.987
30	6.22	373	0.999	0.001	0.73	7.98	0.714
50	1.38	336	0.997	0.004	0.59	8.28	0.863

adsorption in a given concentration range over adsorbent, was also evaluated from the relation,

$$R_L = \frac{1}{1 + K_L C_0} \quad (7)$$

where C_0 is the initial dye concentration (mg/L) [69]. Ho and McKay [70] established that (1) $0 < R_L < 1$ for favorable adsorption; (2) $R_L > 1$ for unfavorable adsorption; (3) $R_L = 1$ for linear adsorption; and (4) $R_L = 0$ for irreversible adsorption.

The Freundlich isotherm is expressed by the following equation,

$$Q_e = K_F C_e^{1/n} \quad (8)$$

where K_F and *n* are the Freundlich constants. The value of *n* quantifies the favorability of adsorption and the degree of heterogeneity of the adsorbent surface. The cases of $n = 1$ and $n > 1$ correspond to linear and favorable adsorptions, respectively, and the case of $n < 1$ indicates unfavorable adsorption. Table 5 summarizes the correlation coefficients (R^2) of the Langmuir (Fig. 10B) and Freundlich isotherms (Figure S3 in Supporting information) of FTC-*x* based on the experimental data. The R^2 value for the Langmuir isotherm model showed a better fit with the adsorption data than the Freundlich isotherm model, suggesting MB adsorption on the FTC-*x* surface via monolayer adsorption process. $R_L < 1$ signifies favorable adsorption of MB for the initial MB concentration of 50–350 mg/L.

The FTC-*x* materials exhibited much higher saturated adsorption capacities than most of conventional adsorbents such as activated carbon [48]. MB is a type of cationic dye which can be adsorbed easily by electrostatic forces on negatively charged surfaces. It is observed that —COOH functionalization significantly enhanced the dye adsorption as compared to FTC-0 (without —COOH functionality). The enhancement is believed to be caused by the favored interfacial interaction between the dye and the adsorbent. The —COOH functionalized FTC-*x* will not only provide multiple accessible reactive sites due to the interconnected 3D structure, but also induce stronger electrostatic attractions. The highest adsorption capacity of 374 mg/g was obtained for FTC-30 at pH = 9, which was much larger than those of the MB onto most of conventional adsorbents such as activated carbon (80–300 mg/g) [48] and the reported carboxylic acid functionalized mesoporous silica (159 mg/g) [47]. Although FTC-50 exhibits the maximum amount of —COOH, its less ordered structure with lower surface area inhibits the effective adsorption. The overall high adsorption capacity of FTC-*x* can be attributed to its high surface area, high pore volume, cage-type structure and electrostatic attraction between the negatively charged carboxylate group and the cationic dye.

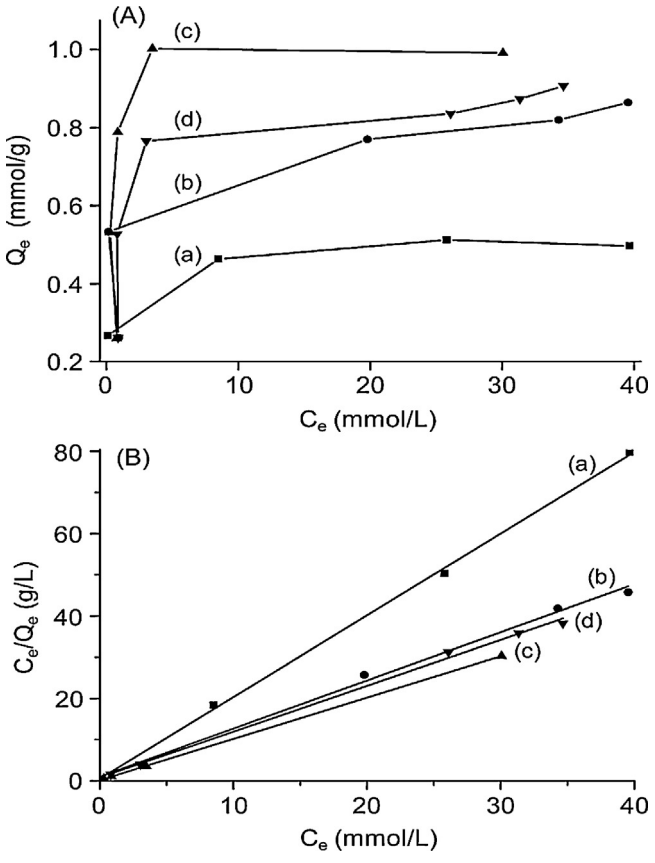

Fig. 10. (A) Effect of initial concentration on the MB adsorption onto (a) FTC-0, (b) FTC-10, (c) FTC-30, and (d) FTC-50 at pH = 9; (B) Langmuir isotherm plot.

3.6. Reuse of the adsorbent

Desorption studies help to elucidate the nature of adsorption and recycling of the used adsorbent and the dye. In order to evaluate the possibility of regeneration of the adsorbent, desorption experiments were performed by washing the dye adsorbed adsorbent in the HCl solution. The quick desorption of the adsorbed dye in the HCl solution suggested that the adsorbate was attached to the adsorbent through chemisorption. Moreover, easy protonation of —COOH group at low pH is beneficial to release the dye molecules quickly. The regenerated adsorbents were treated with de-ionized water to neutralize and dried at 70 °C overnight and then used for removal of MB in the succeeding cycles. The desorption experiments were repeated up to five cycles and the removal efficiency in each cycle is shown in Fig. 11. The removal efficiency was more than 99% after use for five times, suggesting the good quality of the prepared sample.

3.7. FTC-x as antidote for PQ intoxication

Since the pH value of body blood is close to 7.4, the toxicity removal efficiency of FTC-*x* ($x = 0$–50) were evaluated by measuring their capacities to remove PQ in aqueous solutions at pH 7.0 and the results are shown in Fig. 12. Interestingly, the —COOH functionalized FTC-*x* shows PQ removal efficiency of 45–60%, which is around 25% higher than the sample without —COOH loading. The removal yield reached the maximum value of 60% as the CES content is increased up to 50%. As seen in Fig. 12, there is only slight difference of removal efficiency between FTC-10 and FTC-30. Presumably, the chosen pH value is not the optimum condition for the effective adsorption, as in the case of MB adsorption. PQ removal

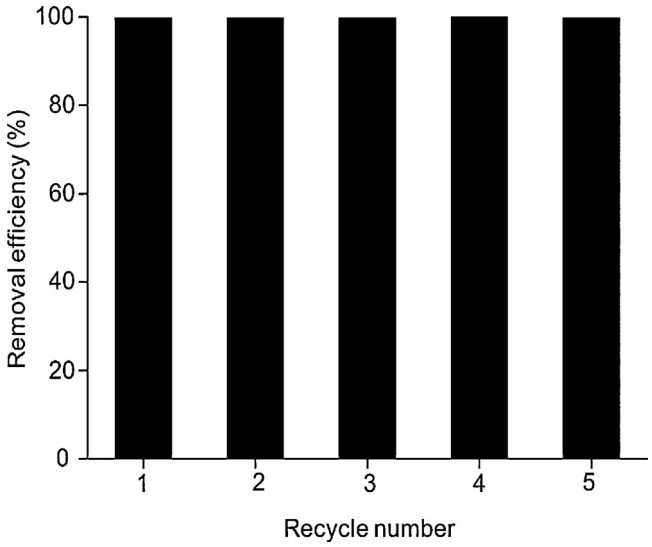

Fig. 11. Recycle of FTC-30.

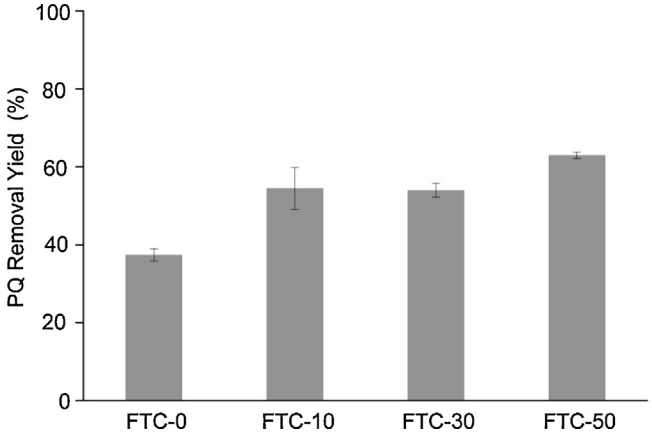

Fig. 12. PQ adsorption onto FTC-*x* at pH = 7.

efficiency of FTC-30 was studied in the pH range of 2–9 and results are shown in Figure S4 (Supporting information). The PQ removal efficiency was negligible at pH 2, probably due to the net positive charge in the adsorption system, owing to the presence of H_3O^+ ions. It is known that PQ reacts as an electron acceptor in redox and radical reaction. At a low pH value, the net positive charge in the adsorption system competes with PQ, resulting in lower PQ adsorption. As the —COOH groups deprotonated at high pH, the adsorbent can adsorb more PQ due to the electrostatic force of attraction between cationic PQ and negatively charged carboxylate groups. Nevertheless, it is noteworthy noticing that charcoal can statistically reduce only around 35% of the absorbed PQ in animal bodies according to a recent report on animal trial data [71]. The present findings can open an auxiliary avenue in the development of a novel filter type for the treatment of poisoned patients in clinical trials, e.g., hemodialysis, at the pH value in bodies.

4. Conclusions

Synthesis of highly ordered FDU-12 type mesoporous silicas functionalized with carboxylic acid groups and their applications as adsorbents for removal of methylene blue and paraquat from aqueous solution are demonstrated. The structural ordering and textural properties of the materials is significantly influenced as the —COOH content is increased up to 40%. The —COOH functionalized cubic mesoporous silica showed a maximum adsorption capacity of 374 mg/g for MB, which is two times higher than that of the pure analog without the organic functionality. The —COOH functional groups introduce negative charged on the mesopore surface, which created strong electrostatic interactions between the cationic adsorbates and the adsorbent. The present results demonstrate that the large pore —COOH functionalized cubic mesoporous silicas are promising candidates for removing pollutants and herbicides from aqueous solutions in environmental and clinical applications.

Acknowledgement

The financial support of this work by the National Science Council of Taiwan is gratefully acknowledged.

Appendix A. Supplementary data

Supplementary data associated with this article can be found, in the online version, at http://dx.doi.org/10.1016/j.apcatb.2013.06.018.

References

[1] J.Y. Ying, C.P. Mehnert, M.S. Wong, Angewandte Chemie International Edition 38 (1999) 56–77.
[2] F. Schüth, Chemistry of Materials 13 (2001) 3184–3195.
[3] F. Schüth, W. Schmidt, Advanced Materials 14 (2002) 629–638.
[4] A. Stein, Advanced Materials 15 (2003) 763–775.
[5] P. Wang, I.M.C. Lo, Water Research 43 (2009) 3727–3734.
[6] N. Calin, A. Galarneau, T. Cacciaguerra, R. Denoyel, F. Fajula, Comptes Rendus Chimie 13 (2010) 199–206.
[7] C.M.A. Parlett, D.W. Bruce, N.S. Hondow, A.F. Lee, K. Wilson, ACS Catalysis 1 (2011) 636–640.
[8] E. Li, V. Rudolph, Energy and Fuels 22 (2007) 145–149.
[9] Y. Lü, G. Lu, Y. Wang, Y. Guo, Z. Zhang, X. Liu, Advanced Functional Materials 17 (2007) 2160–2166.
[10] J. Fan, C. Yu, F. Gao, J. Lei, B. Tian, L. Wang, Q. Luo, B. Tu, W. Zhou, D. Zhao, Angewandte Chemie International Edition 42 (2003) 3146–3150.
[11] F. Kleitz, D. Liu, G.M. Anilkumar, I. Park, L.A. Solovyov, A.N. Shmakov, R. Ryoo, Journal of Physical Chemistry B 107 (2003) 14296–14300.
[12] J.R. Matos, M. Kruk, L.P. Mercuri, M. Jaroniec, L. Zhao, T. Kamiyama, O. Terasaki, T.J. Pinnavaia, Y. Liu, Journal of the American Chemical Society 125 (2003) 821–829.
[13] Y. Sakamoto, I. Díaz, O. Terasaki, D. Zhao, J. Pérez-Pariente, J.M. Kim, G.D. Stucky, Journal of Physical Chemistry B 106 (2002) 3118–3123.
[14] H.-M. Kao, P.-C. Chang, J.-D. Wu, A.S.T. Chiang, C.-H. Lee, Microporous and Mesoporous Materials 97 (2006) 9–20.
[15] G.J.A.A. Soler-Illia, C. Sanchez, B. Lebeau, J. Patarin, Chemical Reviews 102 (2002) 4093–4138.
[16] H. Yoshitake, Journal of Materials Chemistry 20 (2010) 4537–4550.
[17] A. Walcarius, L. Mercier, Journal of Materials Chemistry 20 (2010) 4478–4511.
[18] B. Rác, M. Nagy, I. Pálinko, A. Molna, Applied Catalysis A: General 316 (2007) 152–159.
[19] X.Y. Hao, Y.Q. Zhang, J.W. Wang, W. Zhou, C. Zhang, S. Liu, Microporous and Mesoporous Materials 88 (2006) 38–47.
[20] Q. Yang, J. Liu, J. Yang, M.P. Kapoor, S. Inagaki, C. Li, Journal of Catalysis 228 (2004) 265–272.
[21] X. Feng, G.E. Fryxell, L.-Q. Wang, A.Y. Kim, J. Liu, K.M. Kemner, Science 276 (1997) 923–926.
[22] J. Brown, L. Mercier, T.J. Pinnavaia, Chemistry Communications (1999) 69–70.
[23] B.G. Trewyn, S. Giri, I.I. Slowing, V.S.-Y. Lin, Chemistry Communications (2007) 3236–3245.
[24] M.E. Davis, Nature 417 (2002) 813–821.
[25] T. Yamamoto, S.-I. Kim, J. Chaichanawong, E. Apiluck, T. Ohmori, Applied Catalysis B: Environmental 88 (2009) 455–461.
[26] F.D. Paolis, J. Kukkonen, Chemosphere 34 (1997) 1693–1704.
[27] World Health Organization and UNICEF (2005) Water for life: Making it happen. ISBN 9241562935.
[28] N. Sapawe, A.A. Jalil, S. Triwahyono, S.H. Adam, N.F. Jaafar, M.A.H. Satar, Applied Catalysis B: Environmental 125 (2012) 311–323.
[29] A.R. Khataee, M. Zarei, R. Ordikhani-Seyedlar, Journal of Molecular Catalysis A: Chemical 338 (2011) 84–91.
[30] I.K. Konstantinou, T.A. Albanis, Applied Catalysis B: Environmental 49 (2004) 1–14.
[31] V. Eskizeybek, F. Sarı, H. Gulce, A. Gulce, A. Avcı, Applied Catalysis B: Environmental 119–120 (2012) 197–206.

[32] T.R. Roberts, J.S. Dyson, M.C.G. Lane, Journal of Agricultural and Food Chemistry 50 (2002) 3623–3631.
[33] M. Eddleston, E. Juszczak, N.A. Buckley, L. Senarathna, F. Mohamed, W. Dissanayake, A. Hittarage, S. Azher, K. Jeganathan, S. Jayamanne, M.H.R. Sheriff, D.A. Warrell, The Lancet 371 (2008) 579–587.
[34] R.H. Bromilow, Pest Management Science 60 (2004) 340–349.
[35] A.A. Zagorodni, Ion Exchange Materials: Properties and Applications, Amsterdam, Elsevier, 2006.
[36] B.V. Bruggen, C. Vandecasteele, Environmental Pollution 122 (2003) 435–445.
[37] L.K. Posey, M.G. Viegas, A.J. Boucher, C. Wang, K.R. Stambaugh, M.M. Smith, B.G. Carpenter, B.L. Bridges, S.E. Baker, D.A. Perry, Journal of Physical Chemistry C 111 (2007) 12352–12360.
[38] C.M. Chen, A.C. Lua, Journal of Toxicology and Environmental Health. Part A 60 (2000) 477–487.
[39] E.N. El Qada, S.J. Allen, G.M. Walker, Chemical Engineering Journal 124 (2006) 103–110.
[40] S.B. Wang, H.T. Li, S.J. Xie, S.L. Liu, L.Y. Xu, Chemosphere 65 (2006) 82–87.
[41] B. Armagan, O. Ozdemir, M. Turan, M.S. Celik, Journal of Chemical Technology and Biotechnology 78 (2003) 725–732.
[42] L.C. Juang, C.C. Wang, C.K. Lee, T.C. Hsu, The Journal of Environmental Management 17 (2007) 29–38.
[43] Y. Dong, B. Lu, S. Zang, J. Zhao, X. Wang, Q. Cai, Journal of Chemical Technology and Biotechnology 86 (2011) 616–619.
[44] Q. Tang, Y. Xu, D. Wu, Y. Sun, Journal of Solid State Chemistry 179 (2006) 1513–1520.
[45] M.C. Bruzzoniti, A. Prelle, C. Sarzanini, B. Onida, S. Fiorilli, E. Garrone, Journal of Separation Science 30 (2007) 2414–2420.
[46] A. Lev, Y.E. Korchev, T.K. Rostovtseva, C.L. Bashford, D.T. Edmonds, C.A. Pasternak, Proceedings of the Royal Society of London B 252 (1993) 187–192.
[47] Z. Yan, S.Y. Tao, J.X. Yin, G.T. Li, Journal of Materials Chemistry 16 (2006) 2347–2353.
[48] K.Y. Ho, G. McKay, K.L. Yeung, Langmuir 19 (2003) 3019–3024.
[49] S.B. Yoon, J.Y. Kim, J.H. Kim, Y.J. Park, K.R. Yoon, S.K. Park, J.S. Yu, Journal of Materials Chemistry 17 (2007) 1758–1761.
[50] H.-Y. Wu, F.-K. Shieh, H.-M. Kao, Y.-W. Chen, J.R. Deka, S.-H. Liao, K.C.-W. Wu, Chemistry: A European Journal 19 (2013) 6358–6367.
[51] W.Q. Shui, J. Fan, P.Y. Yang, C.L. Liu, J.J. Zhai, J. Lei, Y. Yan, D.Y. Zhao, X. Chen, Analytical Chemistry 78 (2006) 4811–4819.
[52] D. Zhao, Q. Huo, J. Feng, B.F. Chmelka, G.D. Stucky, Journal of the American Chemical Society 120 (1998) 6024–6036.
[53] C.-T. Tsai, Y.-C. Pan, C.-C. Ting, S. Vetrivel, A.S.T. Chiang, G.T.K. Fey, H.-M. Kao, Chemical Communication (2009) 5018–5020.
[54] K.S.W. Sing, D.H. Everett, R.A.W. Haul, L. Moscou, R.A. Pierotti, J. Rouquerol, T. Siemieniewska, Pure and Applied Chemistry 57 (1985) 603–619.
[55] J. Jiu, K. Kurumada, F. Wang, L. Pei, Materials Chemistry and Physics 86 (2004) 435–439.
[56] C.-S. Chen, C.-C. Chen, C.-T. Chen, H.-M. Kao, Chemical Communications 47 (2011) 2288–2290.
[57] A. El Kadib, P. Hesemann, K. Molvinger, J. Brandner, C. Biolley, P. Gaveau, J.J.E. Moreau, D. Brunel, Journal of the American Chemical Society 131 (2009) 2882–2892.
[58] M. Alkan, M. Dogan, Y. Turhan, O. Demirbas, P. Turan, Chemical Engineering Journal 139 (2008) 213–223.
[59] C. Duran, D. Ozdes, A. Gundogdu, H.B. Senturk, Journal of Chemical and Engineering Data 56 (2011) 2136–2147.
[60] S. Lagergren, Kungliga. Svenska Vetenskapsakademiens. Handlingar 24 (1898) 1–39.
[61] Y.S. Ho, G. McKay, Process Biochemistry 34 (1999) 451–465.
[62] W.J. Weber Jr., J.C. Morris, Journal of the Sanitary Engineering Division, American Society of Civil Engineers 89 (1963) 31–60.
[63] M. Ghaedi, A. Hassanzadeh, S.N. Kokhdan, Journal of Chemical and Engineering Data 56 (2011) 2511–2520.
[64] O.G. Apul, T. Shao, S.J. Zhang, T. Karanfil, Environmental Toxicology and Chemistry 31 (2012) 73–78.
[65] M. Dogan, H. Abak, M. Alkan, Journal of Hazardous Materials 164 (2009) 172–181.
[66] Y.S. Al-Degs, M.I. El-Barghouthi, A.A. Issa, M.A. Khraisheh, G.M. Walker, Water Research 40 (2006) 2645–2658.
[67] I. Langmuir, Journal of the American Chemical Society 40 (1918) 1361–1403.
[68] H.M.F. Freundlich, The Journal of Physical Chemistry 57 (1906) 385–4712.
[69] T.W. Weber, P.K. Chakravorti, J. Am. Inst. Chem. Engrs. 20 (1974) 228–252.
[70] Y.S. Ho, G. McKay, Chemical Engineering Journal 70 (1998) 115–124.
[71] S.Z. Idid, C.Y. Lee, Clinical and Experimental Pharmacology and Physiology 23 (1996) 679–681.